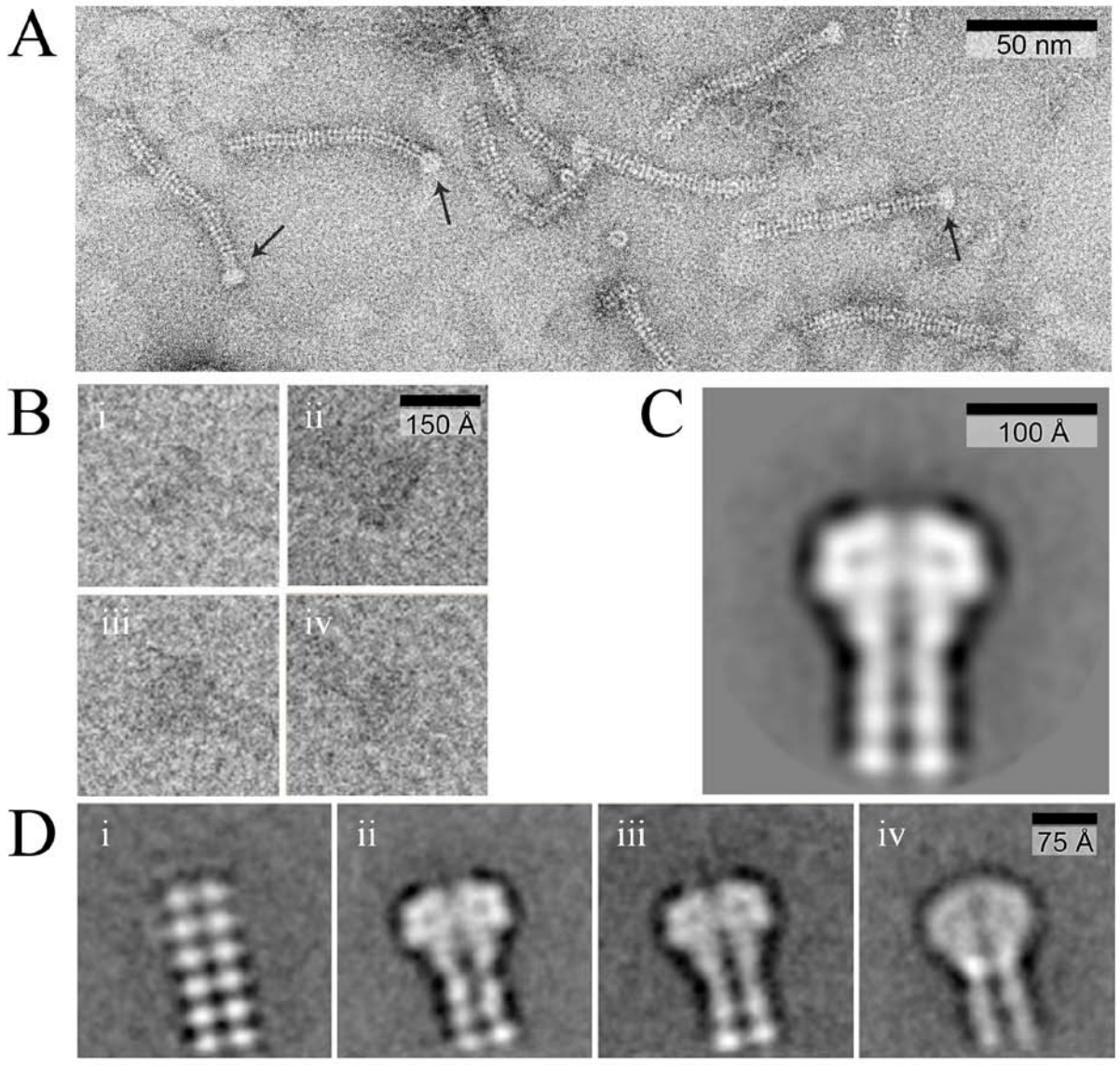

Figure 1. **Negative stain EM of Bacteriophage λ. A,** Section from a micrograph of separated heads and tails of Phage λ stained with 2 % uranyl acetate. Due to the length of the tails, they adopt a preferred orientation on the grid. **B,** Sample of the selected raw particle images of the connector region with a bit of the tail region. The high noise in the particle images requires 2-D averaging with other raw particles of the same view to improve the signal to noise ratio. **C,** 2-D average of all selected particles after rotational and translational alignment. D, Four class averages showing different views of Phage λ connector. The class average on the far left shows tails without connector regions, and the class average on the far right a tilted view of the connector.

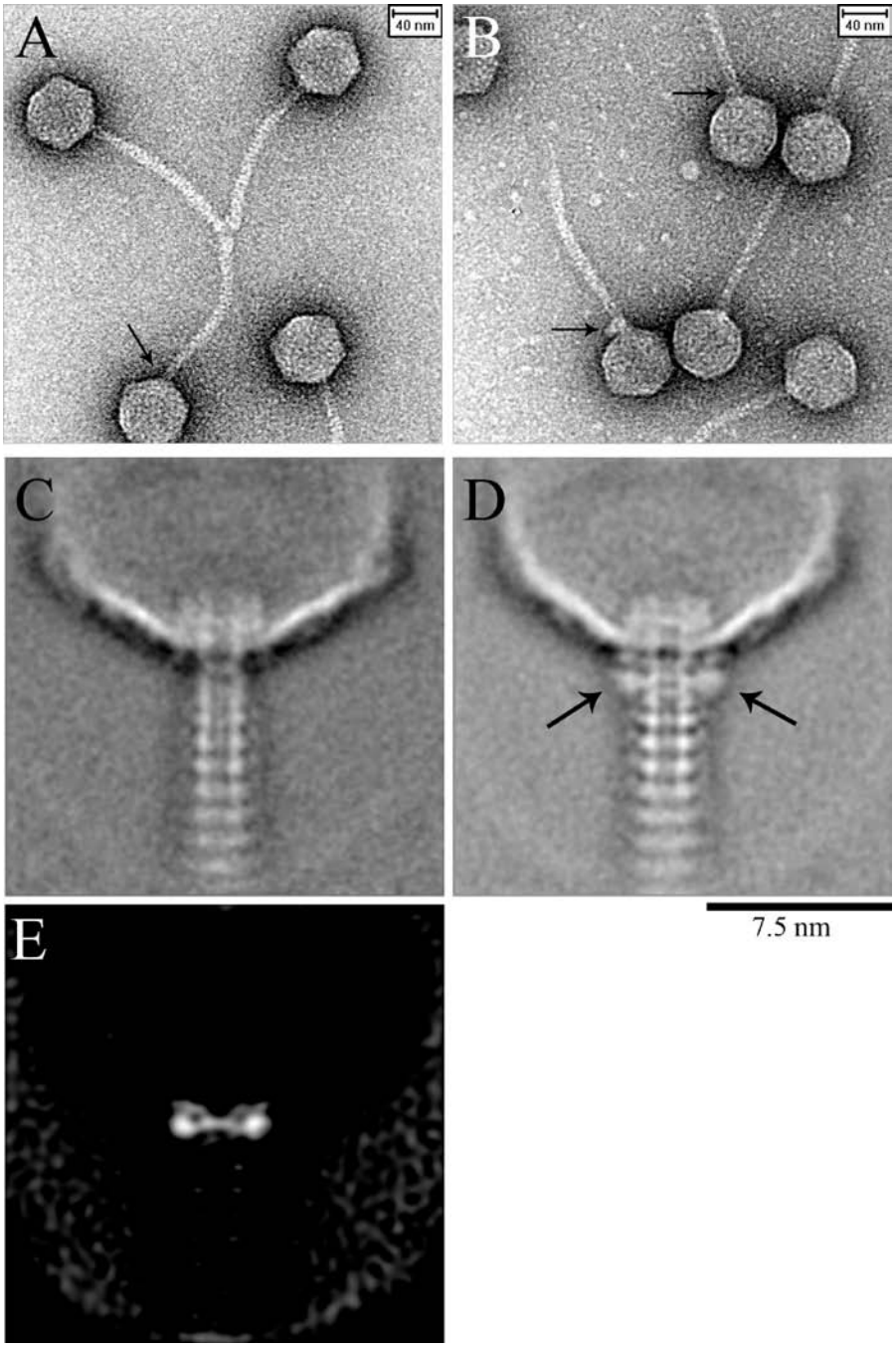

Figure 2. Negative stain EM of Maltose binding protein genetically attached to phage λ's gpW subunit. A, CCD image of wildtype Phage λ in 2 % uranyl acetate. A single black arrow points to the connector region. **B,** CCD images of Phage λ with maltose binding protein (MBP) fused to gpW in 2 % uranyl acetate. Black arrows point to the connector region. **C,** 2-D average of wildtype Phage λ in 2 % uranyl acetate. The connector can be seen at one vertex of the capsid. **D,** 2-D average of Phage λ with MBP attached to gpW. The arrows point to the additional densities surrounding the connector region. **E,** Difference map produced by subtracting the 2-D average of wildtype Phage λ (**C)** from the 2-D average of Phage λ with MBP fused to gpW (**D**). The two spherical densities are MBP.

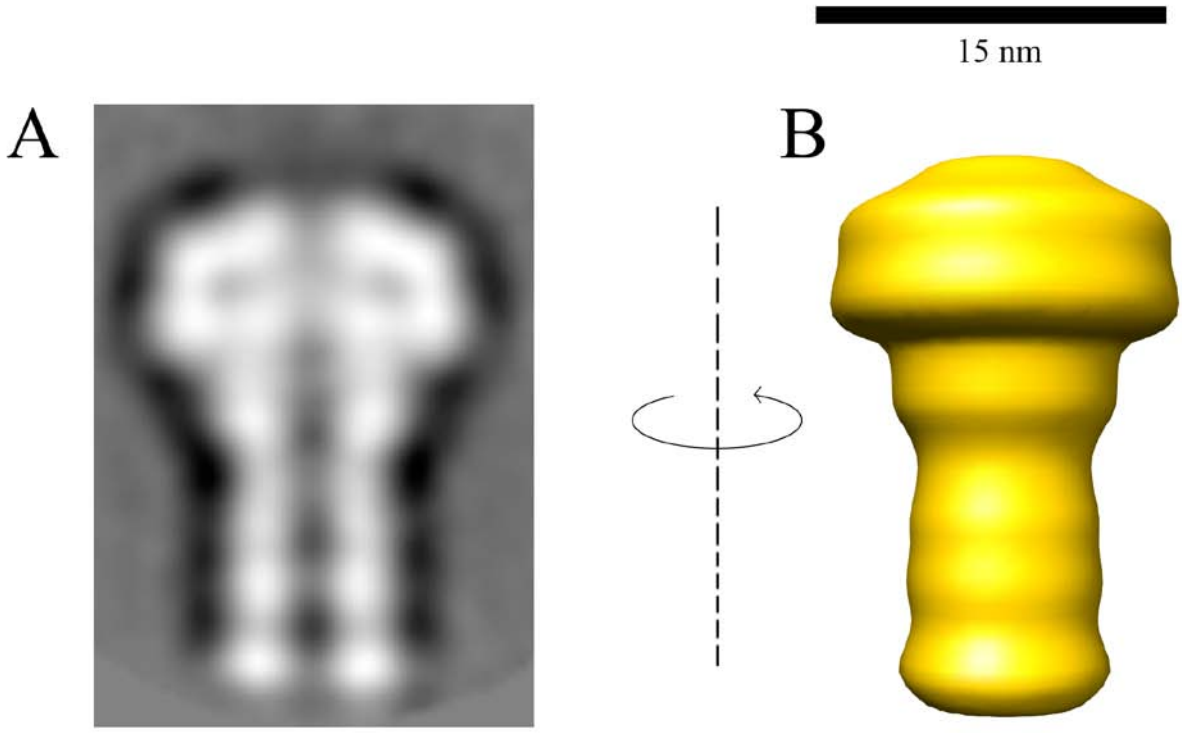

Figure 3. Generating a 3-D initial model from 2-D average. A, An initial model was generated using the cryo-EM 2-D average of the connector region. The 2-D average was replicated 144 times and each replica was assigned a different angle around the long axis of the tail, evenly covering 0° to 360° in increments of 2.5°.

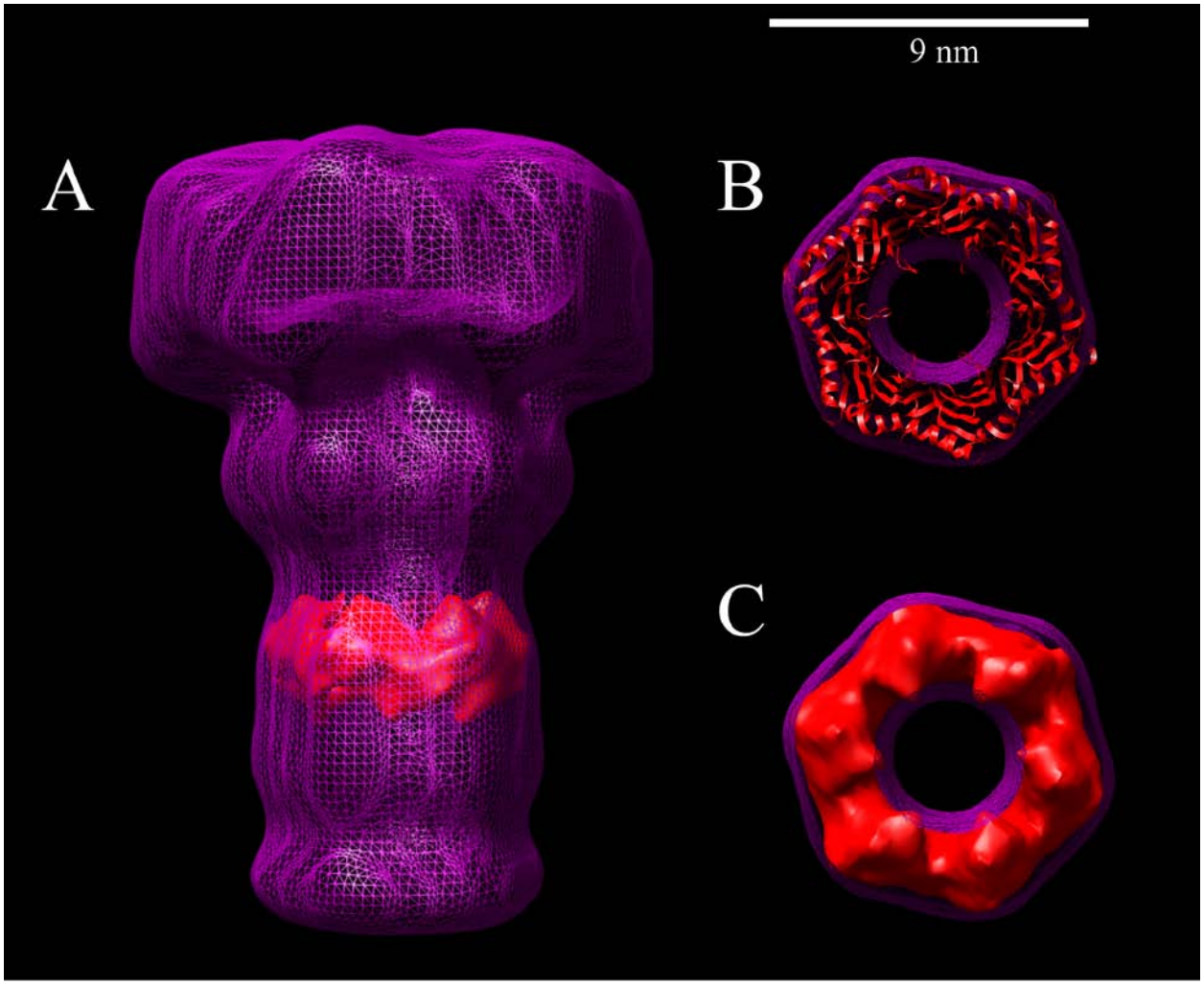

Figure 4. Docking bacteriophage λ`s tail capping protein, gpU, into the 3-D map of the connector region. A, A side view of the 3-D map of the connector region (C_6) displayed as a mesh. An atomic model of oligomeric gpU (REF) was docked inside the 3-D map. Chimera was used to optimize the fit. **B,** Two views of gpU docked inside the tail region of the 3-D map. The atomic model of gpU is displayed as a ribbon on top and as a low-pass filtered 3-D map on the bottom. The general shape and dimensions of the map match the atomic model of gpU well.

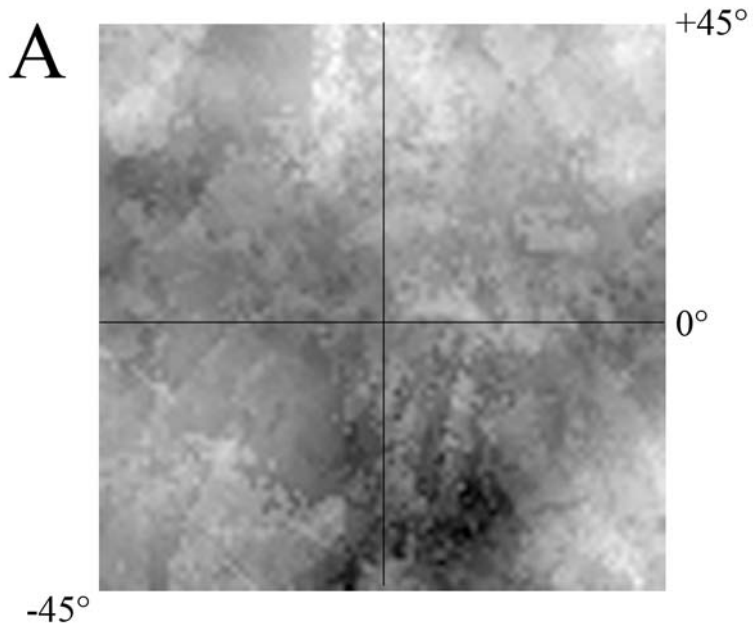

Figure 5. Results of the free hand test on 35 cryo-EM tilt pairs and the CTF-corrected, 6-fold symmetric 3-D map of the connector region of phage λ. A, Dark areas on the map represent low values, while light regions correspond to higher values. A minima is present near the bottom of the plot, at the expected x-rotation of 0° and y-rotation of -30°, indicating that the hand of the model was correct.

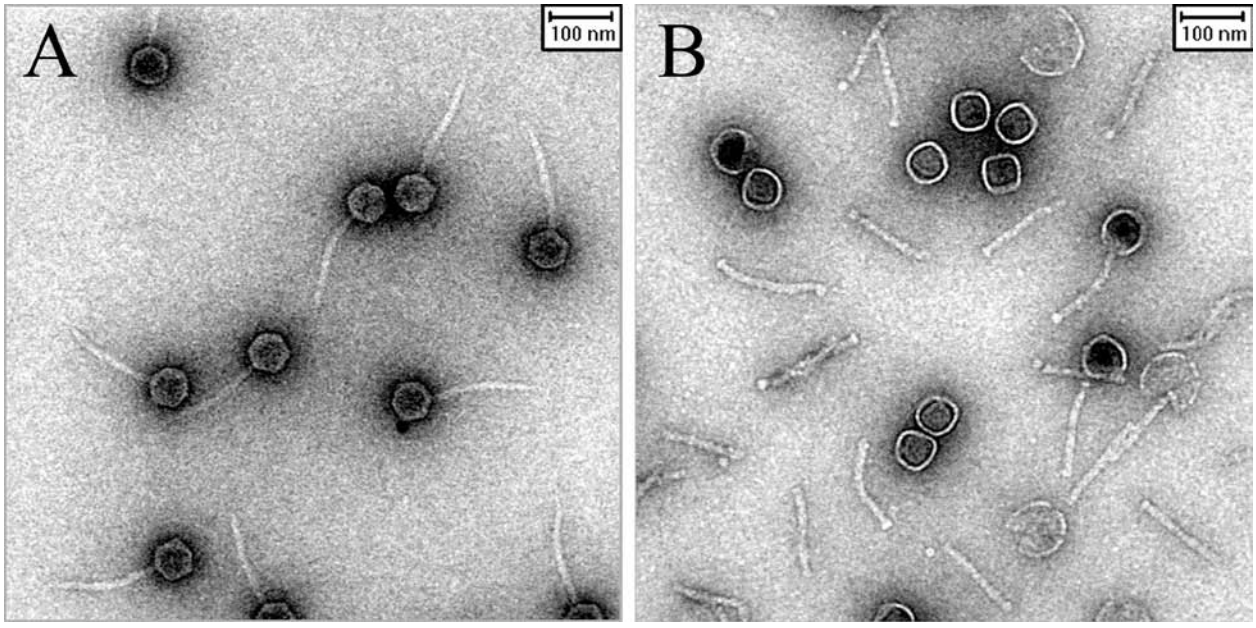

Figure 6. 3 M guanidine hydrochloride separates heads from tails. A, CCD image of wildtype Phage λ imaged in 2% uranyl acetate. **B,** CCD image of wildtype Phage λ in 2 % uranyl acetate after treatment with 3 M guanidine hydrochloride (GuHCl) for 10 min at 55 °C. Heads and tails were separated with the connector remaining attached to the tail. The tail tip was no longer seen after GuHCl treatment.

A

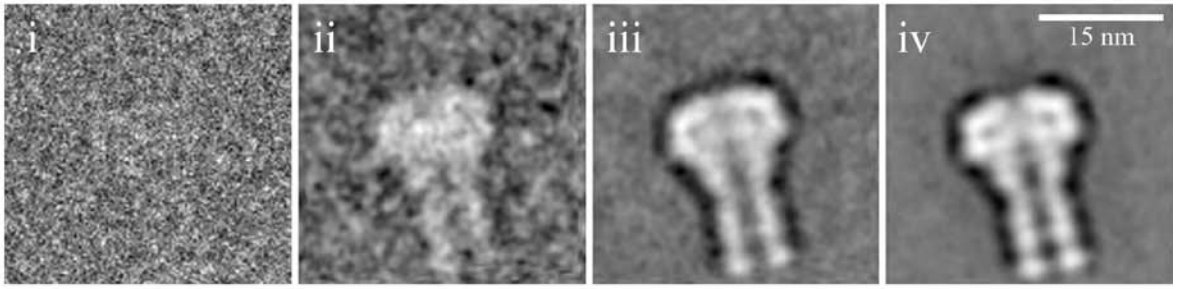

Figure 7. Averaging improves signal-to-noise ratios (SNR). A, Raw 2-D images from cryo-EM are noisy due to the small dose of electrons required to avoid radiation damage to the specimen. The signal can be improved by aligning and averaging particle images with the same view of the specimen, as uncorrelated noise will disappear and signal will remain. Increasing the number of averaged image particles improves the SNR, as shown here for 10 (B), 100 (C), and 1000 (D) images.

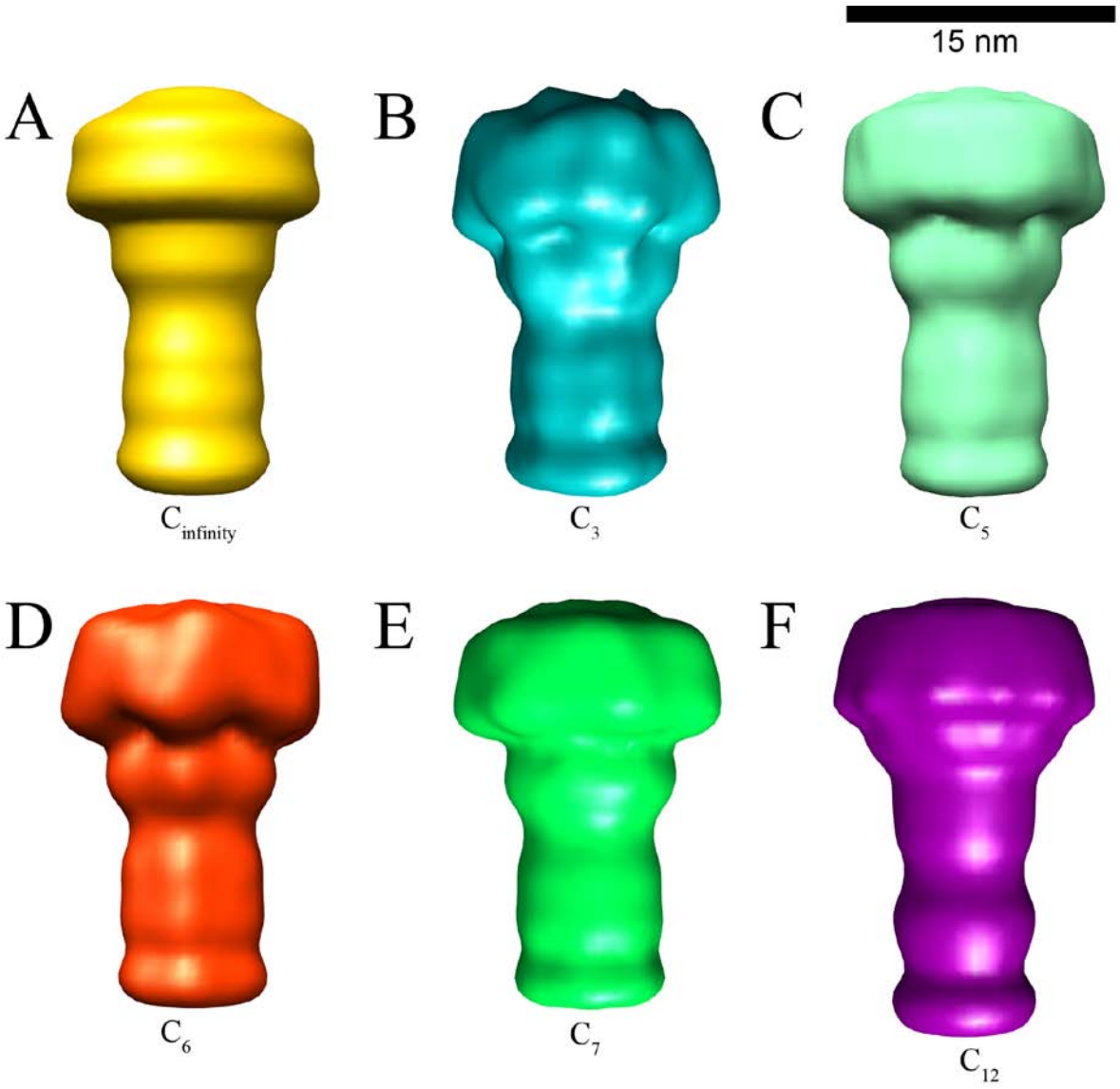

Figure 8. Comparison of the initial model with 3-D maps of different applied symmetries. Five different symmetries were tested in refinement of the initial model (**A**). The resultant final models are shown for C_3 symmetry(**B**), C_5 symetry (**C**), C_6 symmetry (**D**), C_7 symmetry (**E**) and C_{12} symmetry (**F**). The quality of each 3-D map was evaluated with respect to smoothness, appearance of symmetry and any internal distribution of density, and the C_6 map was chosen for further refinement.

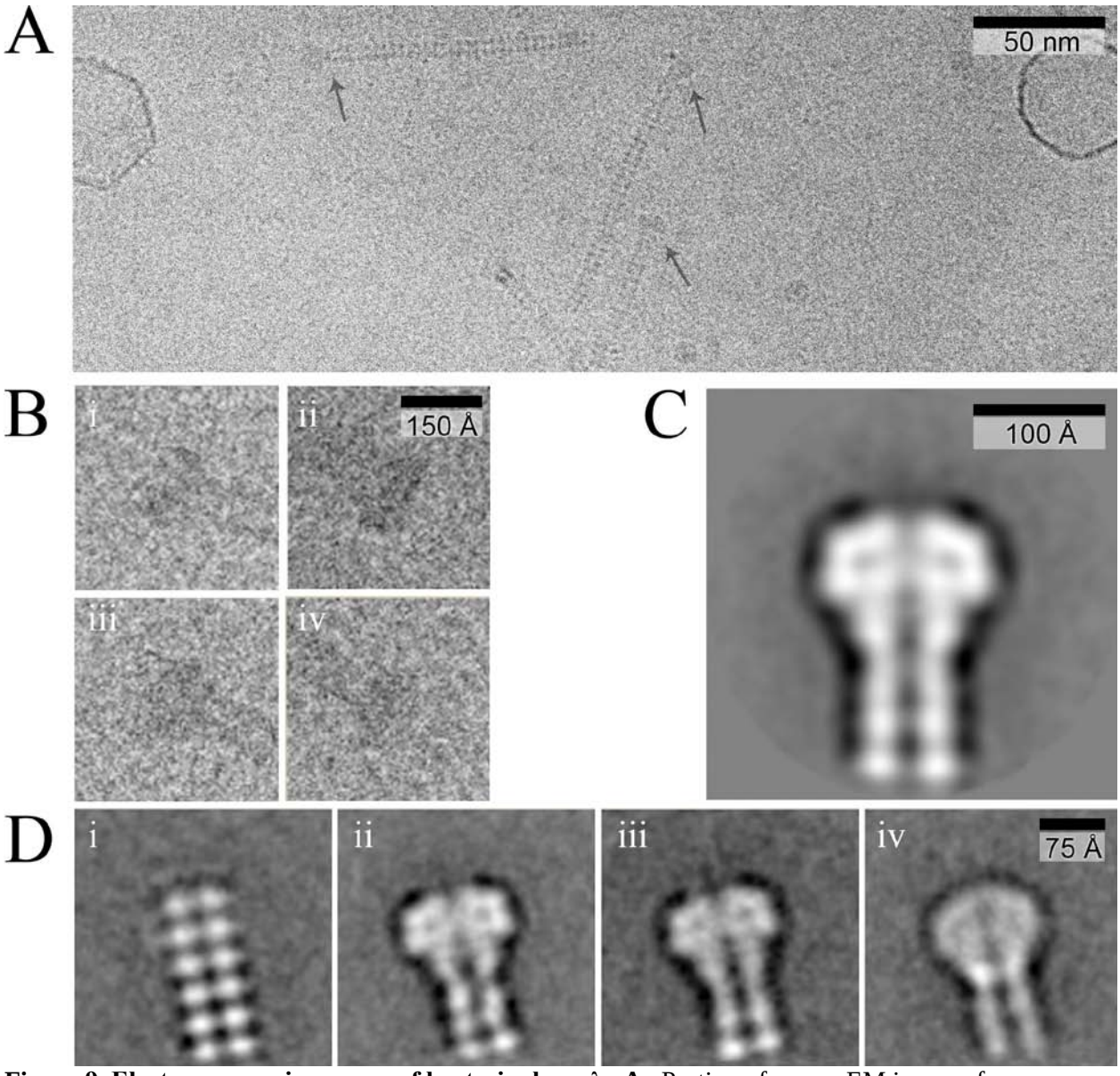

Figure 9. Electron cryomicroscopy of bacteriophage λ. A, Portion of a cryo-EM image of Bacteriophage λ. As with negative stain images, Phage λ is seen with its long axis on the grid. **B,** A sample of the selected raw particle images of the connector region and the attached tail region The high noise in the particle images requires 2-D averaging with other raw particles of the same view to improve the signal to noise ratio.. **C,** 2-D average of all selected particles after rotational and translational alignment. **D,** Four class averages showing different views of Phage λ connector. The class average on the far left shows tails without connector regions, and the class average on the far right a tilted view of the connector.

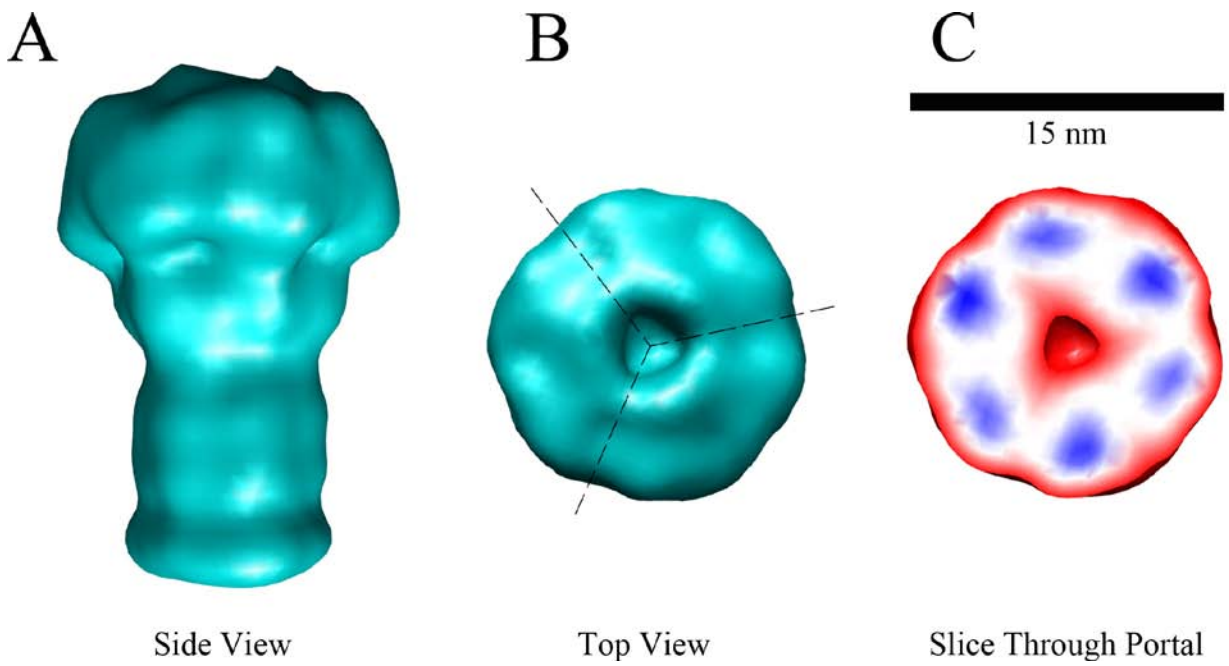

Figure 10. Surface representations of the 3-D map after C_3 symmetry was applied. A, Side and **B,** top view of isosurfaces of the 3-D map with applied 3-fold symmetry. The final 3-D map shows strong 6-fold symmetry in the overall shape and internal density, as seen by a slice through the portal region (C).

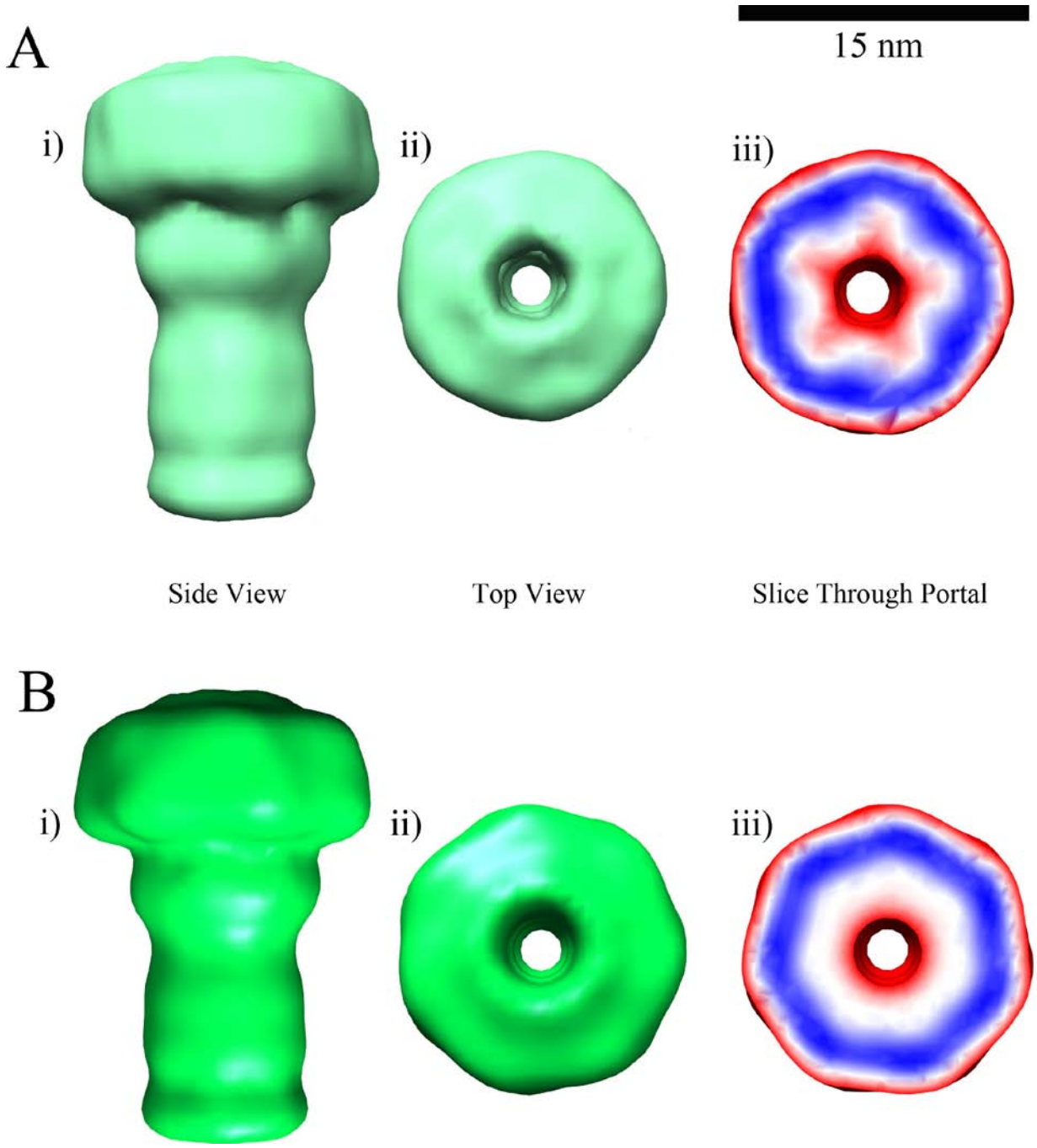

Figure 11. Surface representations of the 3-D map after C_5 and C_7 symmetries were applied. A, (i) Side and (**ii**) top views of the map after application of 5-fold symmetry. The external shape of the model has weak 5-fold symmetry. (**iii**) A slice through the portal region shows an ambiguous distribution of density as individual subunits are not distinguishable. **B, (i)** Side and **(ii)** top view of the map after application of 7-fold symmetry. **(iii)** A slice through the portal region shows density around the perimeter, but does not indicate unique subunits.

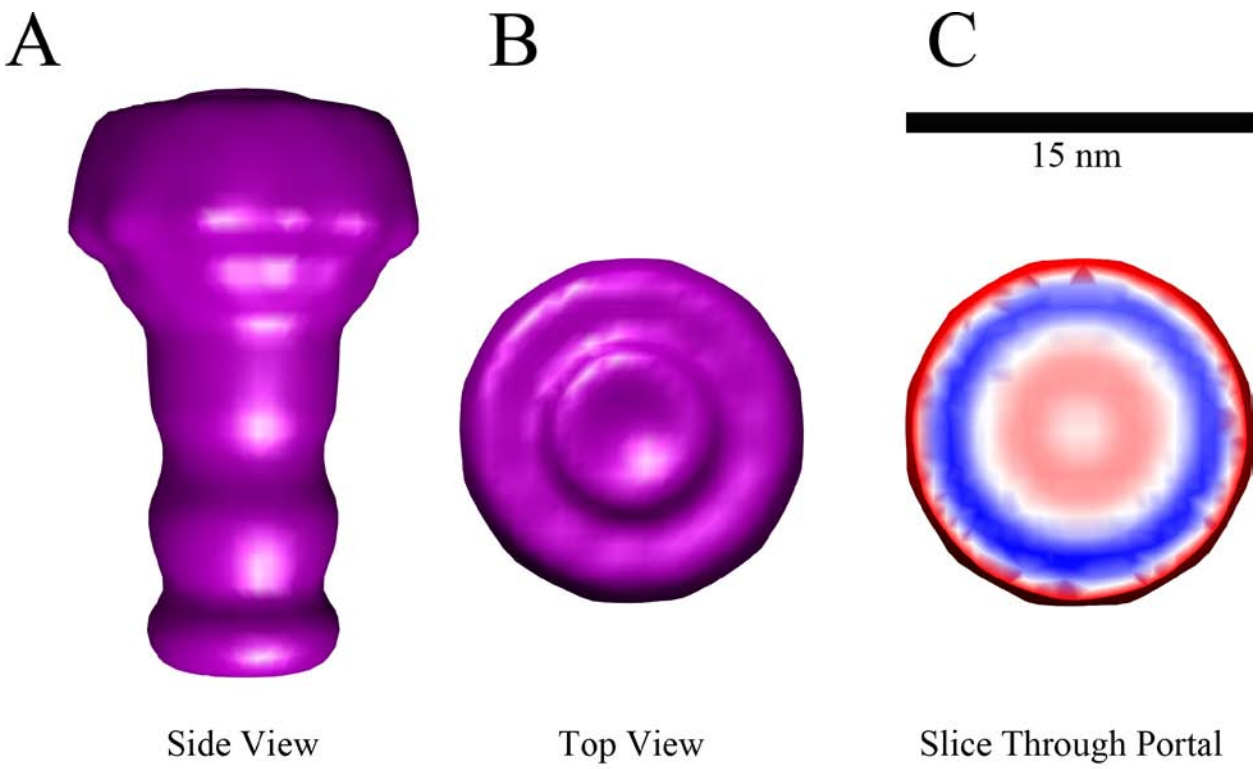

Figure 12. Surface representations of the 3-D map after C_{12} symmetry was applied. A, (i) Side and **(ii)** top views of the map after application of 12-fold symmetry. The tail region was smoothed out entirely and the top view shows minimal 12-fold symmetry. **(iii)** Similarly, internal density showed an even distribution around the perimeter of the portal, but no discernable symmetry or subunit separation.

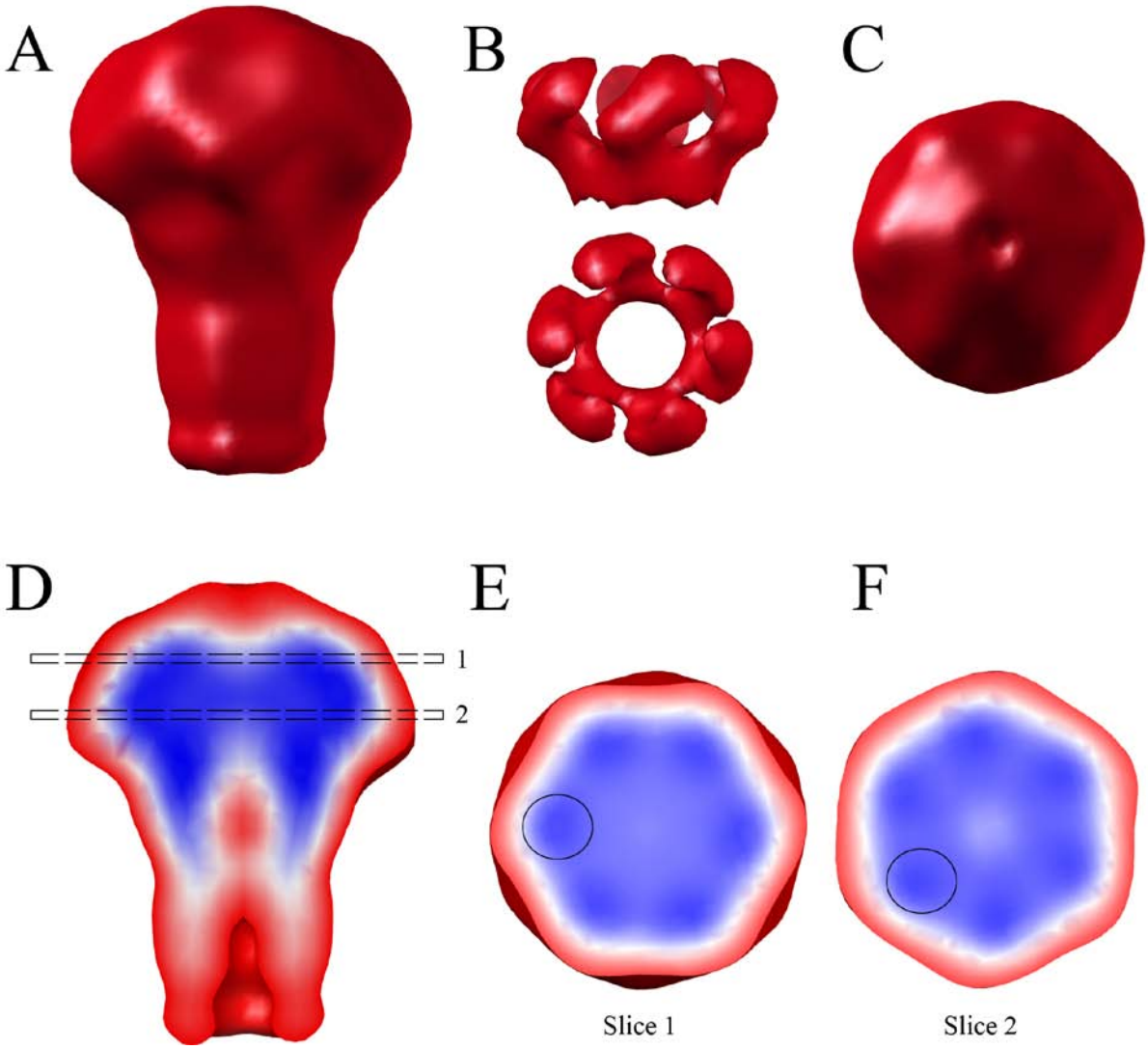

Figure 13. Surface representations of the final 3-D map after refinement with 6-fold symmetry and correction of the contrast transfer function (CTF). A, A side view of 3-D map. The portal is noticeably larger than the non-CTF corrected model (Figure X) and the handedness more apparent. **B,** Side and top view of the portal region at a high-density isosurface. The portal contains a ring of staggered subunits. **C,** A top view of an isosurface of the final 3-D map. **D-F**, Slices through the 3-D map showing the distribution of density inside the portal. **D,** Slice along the long axis of the map, showing a side view of the model. **E** and **F**, Slices were taken through the portal at different positions along the long axis. Both slices show six distinct subunits, one of which is circled in black in each slice. The position of the density rotates as slices are taken from the portal, progressively closer to the tail. The rotation in density position of the same subunit suggests a staggered arrangement of subunits in the portal.

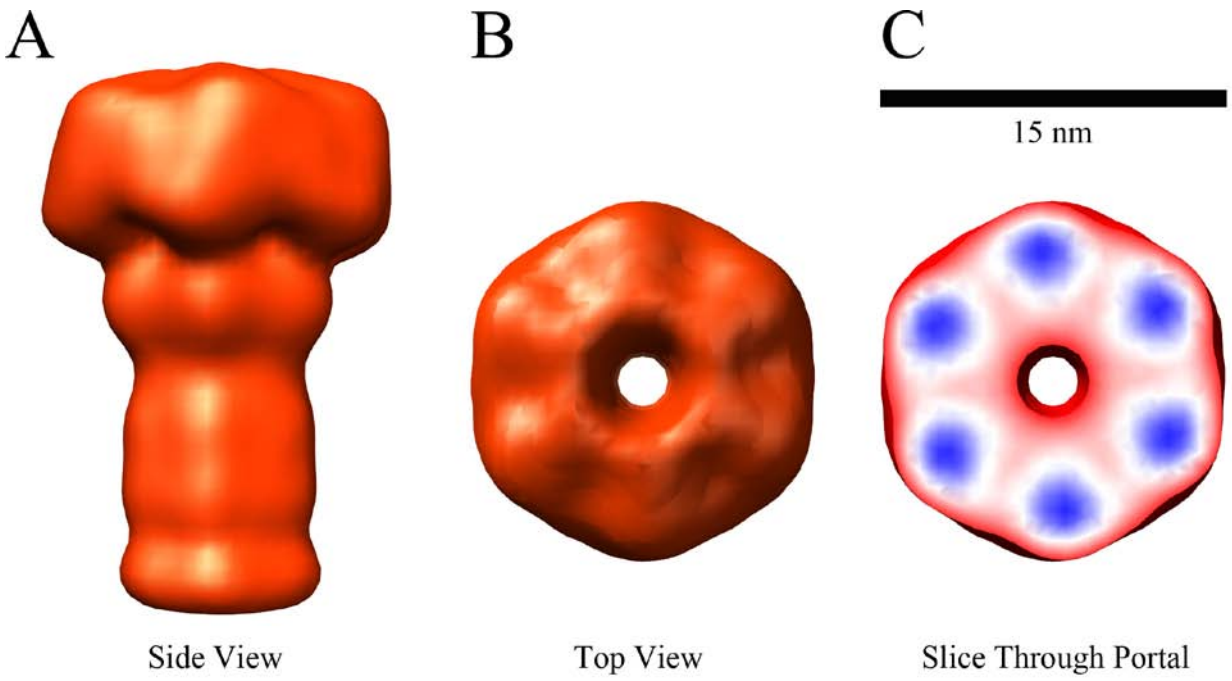

Figure 14. Surface representations of the 3-D map after C_6 symmetry was applied. A, (i) Side and (**ii**) top views of the map after application of 6-fold symmetry. The tail and connector showed strong 6-fold symmetry. The handedness of the connector is beginning to develop in the portal area where the subunits show a vertical "N" shape. **B,** The top view of the connector (portal region) continues to display 6-fold symmetry. **C,** Similarly, internal density revealed 6 distinct regions of high density.